# DNA Cleavage by $^{111}$In-Labeled Oligodeoxyribonucleotides

Valeri N. Karamychev, Igor G. Panyutin, Meyong-Kon Kim, Nhat Le, Chang H. Paik, Jorge A. Carrasquillo, Michael W. Reed, and Ronald D. Neumann

*Department of Nuclear Medicine, Warren G. Magnuson Clinical Center, National Institutes of Health, Bethesda, Maryland; Epoch Pharmaceuticals, Inc., Bothell, Washington; and Novosibirsk Institute of Bioorganic Chemistry, Novosibirsk, Russia*

We studied the fine structure of DNA damage produced by the decay of $^{111}$In incorporated into duplex and triplex DNA strands to evaluate the usefulness of this radionuclide for sequence-specific DNA cleavage. **Methods:** Oligodeoxyribonucleotides (ODNs) were prepared with $^{111}$In attached by diethylenetriaminepentaacetic acid (DTPA) at the 5′ end or 3′ end through a long chemical linker or to an internal nucleotide position through a short linker. Subsequent formation of DNA duplexes and triplexes was confirmed by gel electrophoresis. The $^{111}$In-induced breaks were assayed in denaturing polyacrylamide gel electrophoresis with a single-nucleotide resolution. **Results:** $^{111}$In-labeled oligonucleotides of high specific activity (740–1554 TBq/mmol) were synthesized. The presence of the bulky $^{111}$In-DTPA group did not impede duplex or triplex formation. Localized DNA breaks were observed in all duplexes and triplexes formed. The majority of DNA breaks in duplex formations were located within ±10 nucleotides from the site of attachment of the $^{111}$In-bearing linker. The yield of DNA breaks per decay was 0.38 in a duplex with internally modified ODNs. This is nearly 2 times less than the yield of DNA breaks in the same duplex with $^{125}$I attached through the same linker. The yield of DNA breaks in the pyrimidine and purine strands of DNA triplexes with $^{111}$In attached to the triplex-forming ODNs through the linkers of different length varied from 0.05 to 0.10. The distribution of DNA breaks was wider in comparison with the duplex experiment. The lower yields of breaks per $^{111}$In decay compared with $^{125}$I may be not only the result of lower deposited energy but also of the ionic repulsion of the negatively charged $^{111}$In-DTPA group from the DNA strands. **Conclusion:** We have shown that decay of $^{111}$In produces highly localized DNA breaks. $^{111}$In introduced into triplex- and duplex-forming ODNs through hydrocarbon linkers produces sequence-specific DNA strand breaks with an efficiency nearly comparable with that of $^{125}$I. These findings are supportive of our proposed use of $^{111}$In-ODNs for gene-specific radiotherapy.

**Key Words:** Auger electrons; $^{111}$In; DNA double-strand breaks

**J Nucl Med 2000; 41:1093–1101**

The use of Auger-electron–emitting radionuclides (AEs) for radiotherapy affords a unique opportunity to deliver ionizing radiation not only to specific cells but to specific biomolecules and even to smaller parts of these molecules (*1,2*). The intense emission of low-energy (Auger) electrons and residually charged nuclei that accompany the decay of $^{125}$I, $^{123}$I, and other AEs produces highly dense irradiation within a very short range from the decay site and result in significant damage to adjacent biomolecules (*3–6*).

We proposed targeting disease-causing genes with AEs, thus performing antigene radiotherapy (*7*). For DNA-sequence–specific delivery of AEs, we used synthetic triplex-forming oligodeoxyribonucleotides (TFOs). Unlabeled TFOs were previously proposed for modulation of gene expression in an antigene strategy (*8*). This method was based on the ability of oligopurine and oligopyrimidine (oligodeoxyribonucleotides, ODNs) to bind to polypurine·polypyrimidine sequences in the major groove of DNA in a sequence-specific manner with formation of triple-helical structures (*9,10*). To improve the efficiency of oligonucleotide-mediated antigene therapies, ODNs have also been modified with chemically active groups to cause irreversible damage to the DNA target (*11,12*).

We originally labeled TFOs with $^{125}$I, a well-studied AE (*13*). The decay of $^{125}$I incorporated into DNA as an iododeoxycytidine residue has been shown to result in double-strand breaks that occur within 10 bp around the site of decay (*14*). The decay of $^{125}$I incorporated into a TFO as a iododeoxycytidine residue produces double-strand breaks (DSBs) in the target duplex on triplex formation in vitro with an efficiency close to 1 break per decay (*13*). The combination of the sequence specificity of TFO and the ability of AEs to cause highly localized DNA breaks allows radiation-induced breaks to be confined to the TFO-targeted gene and to produce minimal damage to the rest of the genome, accomplishing, perhaps, the goal of antigene radiotherapy.

Using $^{125}$I allowed us to test the principle of antigene radiotherapy in vitro, and we demonstrated that $^{125}$I-labeled TFOs are able to produce sequence-specific breaks in purified plasmids and genomic DNA. However, to attempt antigene radiotherapy in vivo, other AEs are required.

$^{111}$In has medium-energy γ-ray emissions, a relatively short half-life (2.8 d), and is bound to various carriers for use in nuclear medicine scintigraphy. $^{111}$In has been incorporated into antisense oligonucleotides to evaluate their use for noninvasive diagnosis of mammary tumors in mice (*15*).

Received May 21, 1999; revision accepted Sep. 14, 1999.

For correspondence or reprints contact: Valeri N. Karamychev, MD, Visiting Fellow, NMD, CC, National Institutes of Health, 10 Center Dr., MSC 1180, Bethesda, MD 20892-1180.

In addition to being a γ emitter, $^{111}$In is an AE with total energy of Auger electrons that is about half that of $^{125}$I (*16*). $^{111}$In bound nonspecifically to plasmid DNA produced more single-strand breaks than nonbound $^{111}$In in solution. The experiments were performed in aqueous solution using $^{111}InCl_3$, in the absence or presence of diethylenetriaminetripentaacetic dianhydride (DTPA dianhydride), a metal chelator that forms a negatively charged In-DTPA complex and uses ionic repulsion to prevent the binding of In to DNA (*17*). However, the fine structure of DNA damage produced by $^{111}$In delivered to DNA in a sequence-specific manner had not yet been examined. Nor was information available regarding the ability of $^{111}$In-labeled ODNs to form DNA triplexes.

In this article we report the sequence-specific DNA breaks produced by decay of $^{111}$In attached to duplex- or TFOs through linkers of various lengths, and we compare our results to those previously obtained with $^{125}$I-ODNs.

## MATERIALS AND METHODS

### Synthesis of Oligodeoxyribonucleotides

ODNs were synthesized on an ABI394 DNA synthesizer (PE Applied Biosystems, Foster City, CA) and purified as described previously (*13*). The structures and sequences of the amine-modified oligonucleotides $NH_2$-ODN-(1-4) are shown in Figure 1A. The 3′-hexanol modification was introduced into ODN-1 and ODN-2 through the use of a hexanol-modified, controlled-pore glass (CPG) support (*18*). The 5-(3-aminopropyl)-2′-deoxyuridine modification was introduced into ODN-1 and ODN-2 using the corresponding phthalimide-protected phosphoramidite (*19*). ODN-3 was modified with 5′-aminohexyl using N-MMT-hexanolamine phosphoroamidite linker (Glen Research, Sterling, VA). The 6-aminohexyl-2-methoxy modification was introduced into ODN-4 using 3′-amino modifier C7 CPG (Glen Research).

### Synthesis of $^{111}$In-ODN-1

*Conjugation of DTPA with Oligodeoxyribonucleotides.* ODN solutions (57–245 μmol/L) were prepared in 0.3–0.5 mol/L sodium bicarbonate (pH 8.4). To these solutions, fresh cyclic DTPA dianhydride (cDTPAA) solutions (27.6–98.2 mg/mL and 0.08–0.28 mmol/mL) prepared in dry dimethyl sulfoxide (DMSO) were added in 3 equal portions at 15-min intervals. The conjugation reaction was continued for 15 min after the last portion of the cDTPAA solution was added. The total concentration of cDTPAA was 280–1260-fold greater than the concentration of ODNs. The DTPA-conjugated ODNs were then purified with spin G-50 columns (5 Prime ↑ 3 Prime Inc., Boulder, CO) prewashed with 0.2 mol/L sodium acetate and 0.02 mol/L sodium citrate buffer (pH, 4.5). The spin column chromatography was repeated several times until free DTPA was completely removed. The concentration of the purified DTPA-ODN conjugates was determined by ultraviolet spectroscopy (Hewlett Packard Co., Gloucester, VA). To determine the percentage of ODN conjugated to DTPA a small fraction of DTPA-ODN conjugates was labeled with [γ-$^{32}$P]-adenosine triphosphate (ATP) using T4 polynucleotide kinase (New England Biolabs, Beverly, MA) following the manufacturer's protocol and

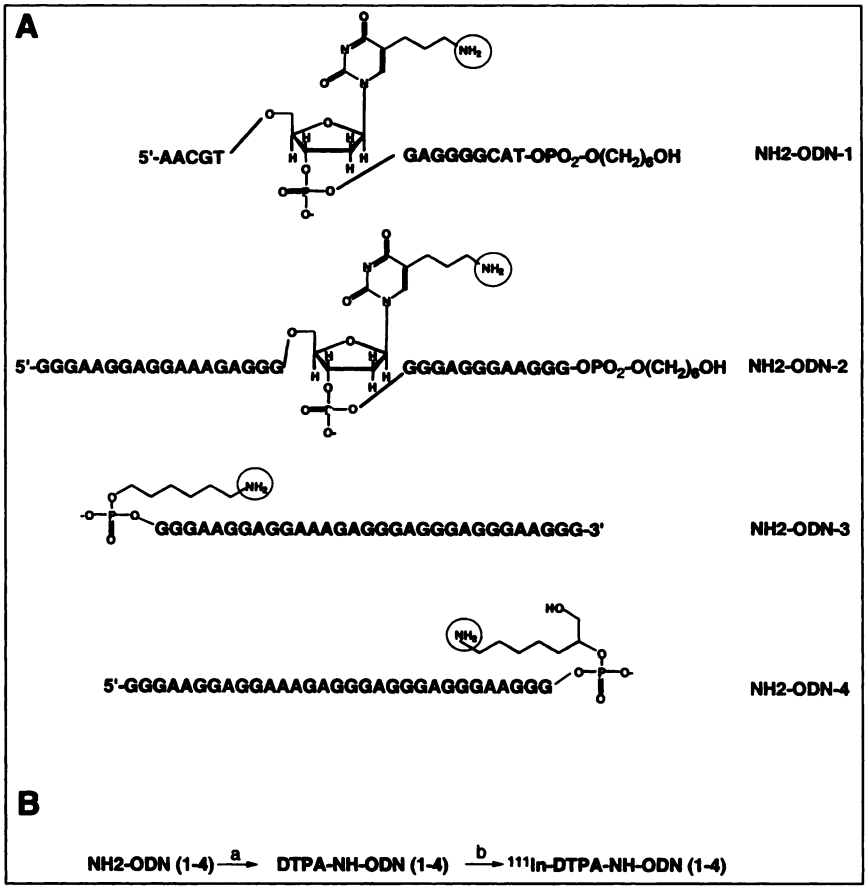


**FIGURE 1.** (A) Sequences of amine-modified oligonucleotides used for synthesis of $^{111}$In-ODN(1-4). (B) Scheme for synthesis of $^{111}$In-ODN(1-4). Reagents: (a) cDTPA, DTPA, (b) $^{111}InCl_3$.

analyzed by denaturating polyacrylamide gel electrophoresis (PAGE). The gel was fixed in 10% acetic acid and dried. The intensity of the bands corresponding to the $^{32}$P-ODN and $^{32}$P-DTPA-ODN were measured with a BAS 1500 BioImaging Analyzer (Fuji, Stamford, CT) as described previously (*13*).

### $^{111}$In Labeling with DTPA Conjugates of Oligodeoxyribonucleotides

An aliquot (1–4 μL) of these conjugates (1.03–4.12 μmol/L) was then radiolabeled with a 15-fold molar excess of $^{111}$In chloride (26–103.6 MBq, 15.5–62 pmol in 2.5–10 μL of 0.05 mol/L HCl) for 1 h at room temperature. The pH of the solutions was adjusted to 4.5 by the addition of 2 mol/L sodium acetate when necessary. The molar excess of free $^{111}$In ion was then quenched by adding 5 mmol/L DTPA and incubating for 10 min. The $^{111}$In-labeling yield was determined by reverse-phase (Rp) thin-layer chromatography (TLC) (5 × 20 cm, eluate 10 mmol/L sodium phosphate [pH, 6.7]; Uniplate; RPS-FAnaltech Inc., Newark, DE) and by size-exclusion high-performance liquid chromatography (HPLC) equipped with a Supelco G2000SW column and an on-line flow radioactivity detector (Bioscan Inc., Washington, DC). The radioactivity on Rp-TLC was scanned with a Bioscan System 300 Imaging Scanner detector (Bioscan Inc.). The radioactivity peaks corresponding to $^{111}$In-DTPA-ODNs and $^{111}$In-DTPA were scraped off from the TLC plate and counted in a γ counter (Packard Co., Downers Grove, IL). The remaining $^{111}$In-labeled products were subjected to the spin column chromatography until $^{111}$In-DTPA was completely removed. The radiochemical purity of the products was confirmed by Rp-TLC and size exclusion as HPLC described above.

### Duplex Preparation

The 42-mer target (ODN-5) was labeled with [γ-$^{32}$P]-ATP using T4 polynucleotide kinase (New England Biolabs), following the manufacturer's protocol. The product was purified on MicroSpin G-50 column (Amersham Pharmacia Biotech Inc., Piscataway, NJ), and its final concentration was estimated to be 200 nmol/L. The $^{32}$P-ODN-5 (0.25 pmol, 1.25 μL) and $^{111}$In-ODN-1 (0.65 pmol, 24 μL, 55 kBq) were annealed at 37°C for 10 min in 1X STE buffer (50 mmol/L Tris HCl [pH, 7.5], 1 mmol/L ethylenediaminetetraacetic acid [EDTA], 150 mmol/L NaCl) followed by slow cooling to 20°C. Formation of the duplexes was confirmed in 20% nondenaturating PAGE. The samples were frozen at −70°C for dose accumulation. Control oligonucleotide $^{32}$P-ODN-5 was subjected to the same freeze, thaw, and denaturation as the duplex.

### Triplex Preparation

The ODN-6 was labeled with [γ-$^{32}$P]-ATP using T4 polynucleotide kinase (New England Biolabs), and the ODN-7 was labeled with [α-$^{32}$P]-deoxyadenosine triphosphate (dATP) using terminal transferase from calf thymus (Boehringer Mannheim, Indianapolis, IN). The products were purified on a MicroSpin G-50 column equilibrated with STE buffer (50 mmol/L Tris HCl [pH 7.5], 1 mmol/L EDTA, 150 mmol/L NaCl), and concentration was estimated to be 0.75 pmol/μL. Fifteen pmol $^{32}$P-ODN-6 and 15 pmol ODN-7 ($D_1$ duplex) or 15 pmol $^{32}$P-ODN-7 and 15 pmol ODN-6 ($D_2$ duplex) were annealed at 75°C for 2 min in 1X Pol buffer (10 mmol/L Tris HCl, pH 7.5, 10 mmol/L $MgCl_2$, 50 mmol/L KCl, 1 mmol/L dithiothreitol [DTT]) followed by slow cooling to room temperature. The labeled duplex was finally purified by 20% nondenaturating PAGE as described previously (*20*), and the final concentration of each was estimated to be 0.1 pmol/μL. To form triplexes, the $D_1$ and $D_2$ duplexes (0.8 pmol, 8 μL each) and $^{111}$In-ODN-2, $^{111}$In-ODN-3, or $^{111}$In-ODN-4 (1.6 pmol, 1.37 MBq, 6 μL) were mixed in 1X binding buffer (50 mmol/L Tris HCl [pH, 8], 10 mmol/L $MgCl_2$, and 1 mmol/L spermidine) in a total volume of 16 μL to form triplexes (T1, $^{111}$In-ODN-2 + $D_1$; T2, $^{111}$In-ODN-2 + $D_2$; T3, $^{111}$In-ODN-3 + D1; T4, $^{111}$In-ODN-3 + $D_2$, T5, $^{111}$In-ODN-4 + D1; T6, $^{111}$In-ODN-4 + $D_2$). The structures of the triplexes are shown in Figure 2. After incubation at 37°C for 24 h, the samples were analyzed by the band shift assay (*21*) in 20% native PAGE in Tris-borate-EDTA containing 5 mmol/L $MgCl_2$. The intensities of the bands, corresponding to the duplexes and triplexes, were measured, and the percentage of radioactivity associated with triplex structures was calculated. The samples were frozen at −70°C for dose accumulation. Control duplexes $D_1$ and $D_2$ were subjected to the same freeze, thaw, and denaturation as triplexes.

### Fragmentation Analysis

After 12 d, the samples were analyzed for fragmentation of the target by 12% denaturing PAGE. Sequencing reactions were performed as described previously (*22*). The gels were fixed in 10% acetic acid and dried. The locations of the bands relative to the sequence of the ODN-5 for duplex and ODN-6 and ODN-7 for triplex were determined by comparison with the Maxam-Gilbert G-sequencing lane. The bands corresponding to the breaks in $^{32}$P-ODN-5 for duplex and $^{32}$P-ODN-6 and $^{32}$P-ODN-7 for triplex were measured using BAS 1500 BioImaging Analyzer software (Fuji) and, after subtraction of the corresponding areas in the blank control ($^{32}$P-ODN-5 for duplex and $D_1$, $D_2$ duplexes for triplexes), expressed as a percentage of the total radioactivity in the lanes, including the top band of undamaged fragment. Data from 3 independent experiments were normalized by the percentage of radioactivity associated with duplex and triplex structures. Then the averages and standard deviations (σ) were calculated (Fig. 3B, Figs. 4 and 5).

## RESULTS

### Oligodeoxyribonucleotide Conjugation and Labeling

The amine-modified ODNs were conjugated with the cyclic anhydride of DTPA as has been described by others (*15,23*) for radiolabeling with $^{111}$In using procedures routine for antibody labeling (*24,25*). The percentage of unconjugated ODN was determined by labeling an aliquot of ODNs with [γ-32P]-ATP before and after conjugation, and the samples were analyzed by denaturing PAGE (Fig. 3A, lines 1 and 2). The DTPA-NH-ODN conjugates migrate slower in the PAGE. In the ODN-1 sample (Fig. 3A, line 2), 90% of the material migrates slower than the unconjugated ODN (Fig. 3A, line 1). Two bands correspond to the products of conjugation (arrows). The lower of the bands, which contains 90% of the conjugated ODN, was assumed to be the expected product. We believe that the upper band is a product of double conjugation. Although the exact chemical nature of these products has not been determined, the PAGE assay allowed optimization of the conditions of conjugation.

To obtain $^{111}$In-DTPA-NH-ODNs with maximum specific activity, a 15-fold molar excess of $^{111}$In-chloride was added to the solution of DTPA-NH-ODNs. The excess of free $^{111}$In ion was quenched by adding DTPA and was removed by several repeated gel filtration chromatographies. PAGE

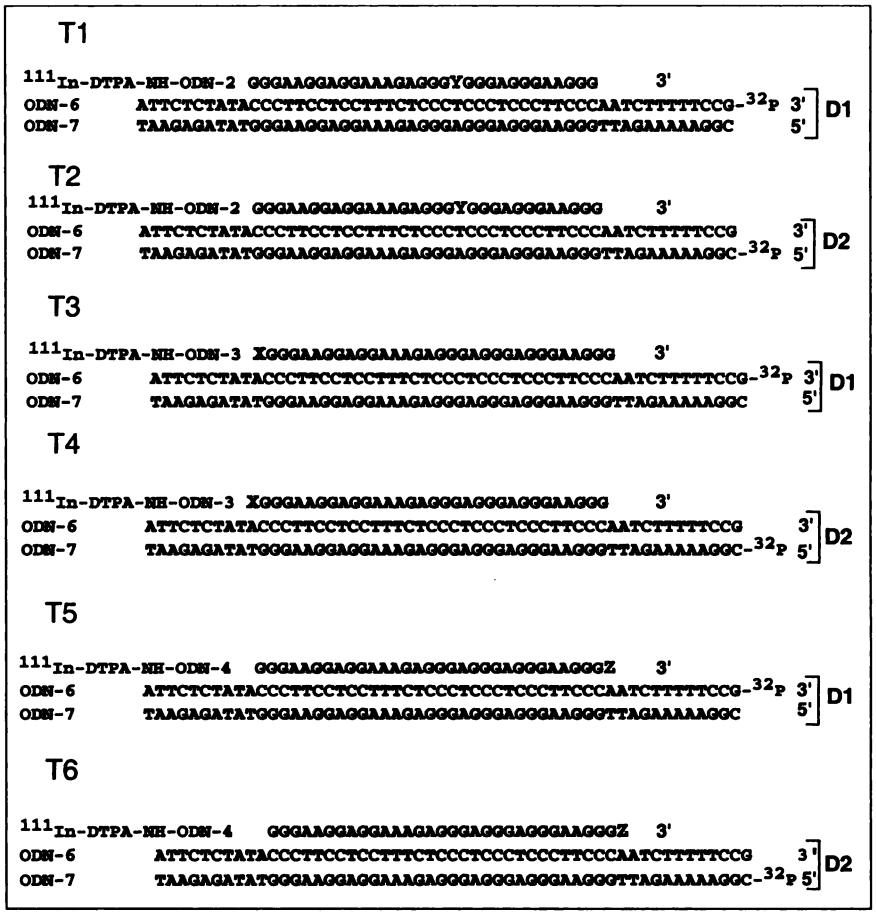


**FIGURE 2.** Sequences of triplexes. X, Y, and Z indicate position of $^{111}$In-labeled residues.

analysis of $^{111}$In-DTPA-NH-ODN-1 is shown in Figure 3A (lane 3). We believe that the lower band is a product of $^{111}$In incorporation into single-DTPA–conjugated ODN, whereas the upper band results from $^{111}$In incorporation into double-DTPA–conjugated ODN (upper of the marked bands on lane 2) The radiochemical purity of the products was confirmed by Rp-TLC, size-exclusion HPLC, and denaturating PAGE as described previously in this article. The measured specific activities of all $^{111}$In-labeled ODNs ranged from 740 to 1554 TBq/mmol.

### Breaks in the Complementary Strand of a Duplex

The $^{111}$In-ODN-1 (Fig. 1) was annealed to complementary ODN-5 to form a duplex (Fig. 3B). The ODN-5 was 5′-end labeled with $^{32}$P for the subsequent breaks analysis in denaturating PAGE. The nondenaturating PAGE analysis of the sample revealed that 95% of the ODN-5 formed duplexes (data not shown). The samples were frozen and kept at −70°C for dose accumulation.

After 12 d of storage, the sample was analyzed for fragmentation by 12% denaturating PAGE as shown in Figure 3A, lane 4. The location of the bands relative to the sequence of the ODN-5 was determined by comparison with the Maxam-Gilbert G-sequencing lane (lane 6). Therefore, a break at a given position indicates the complete removal of the corresponding base (*22*). Bands corresponding to the shorter fragments as a result of the breaks are bracketed (Fig. 3A, lane 4). The intensities of the bands were measured and, after subtraction of the corresponding areas in the blank control ($^{32}$P-ODN-5, lane 5), expressed as a percentage of the total radioactivity in the lanes, including the top band of undamaged fragment. These values are termed frequencies of breaks ($F_i$). The total frequency (F) of $^{111}$In-decay–induced cleavage of $^{32}$P-ODN-5, calculated as the sum of the frequencies of breaks corresponding to individual bases ($F_i$), was 12.6% for the $^{111}$In-duplex. The fraction of $^{111}$In that decayed in N days can be calculated as:

$$1 - 2^{-N/T_{1/2}},$$

where $T_{1/2}$ = 2.8 d and is the half-life of the isotope. Thus, after N = 12 d, 94.9% of the $^{111}$In decayed. Taking into account that the efficiency of incorporation of $^{111}$In into ODN-1 was 36% and that only 95% of ODN-5 was bound to $^{111}$In-ODN-1, we calculated the yield of strand breaks per decay as:

$$B = 0.126/(0.949 \times 0.36 \times 0.95) = 0.38.$$

The bar graph in Figure 3B shows the yields of strand breaks per decay of $^{111}$In and $^{125}$I for individual bases (Bi) (calculated as Bi = Fi × B/F) for the duplex bearing the short internal linker (Fig. 1A) (the data for $^{125}$I-duplex, bearing the same linker, are from Karamychev et al. [*26*]). The maximum of the breaks distribution is shifted 4 bases

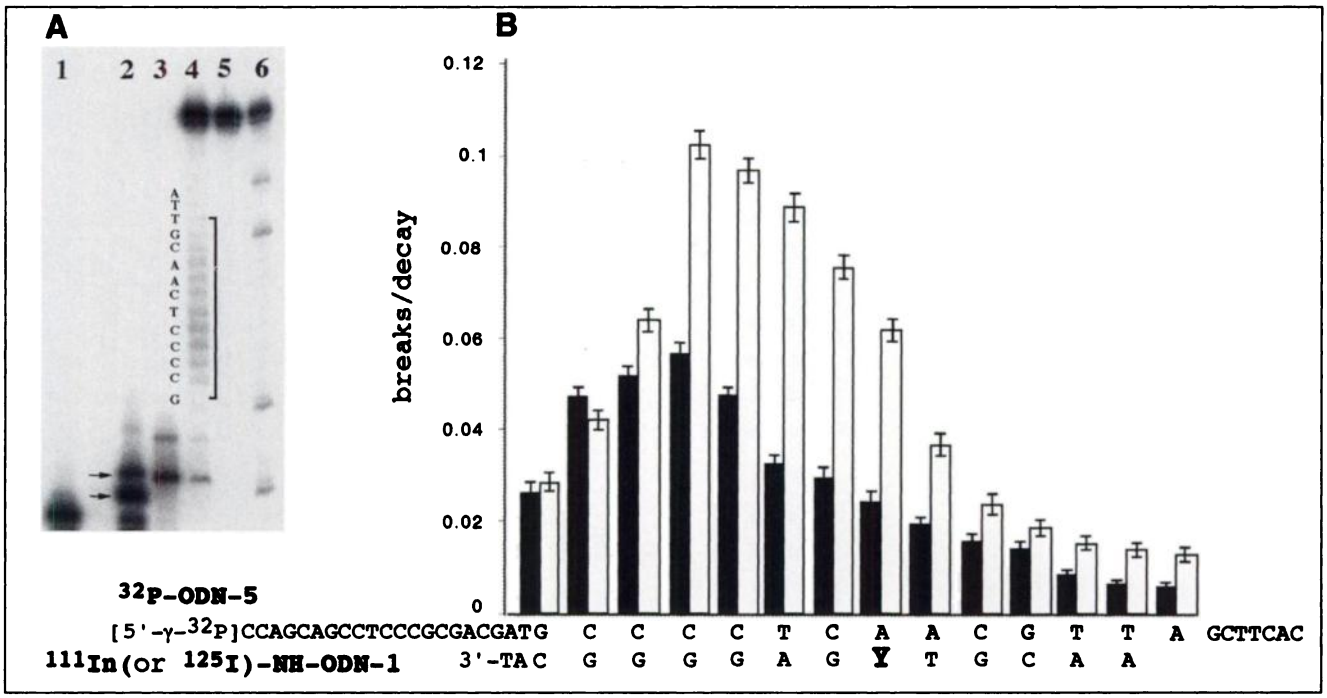


**FIGURE 3.** (A) Analysis of breaks in 12% denaturating PAGE. Lanes: (1) [5′-$^{32}$P]-$NH_2$-ODN-1; (2) [5′-$^{32}$P]-DTPA-NH-ODN-1; (3) $^{111}$In-DTPA-NH-ODN-1; (4) duplex $^{111}$In-DTPA-NH-ODN-1 + $^{32}$P-ODN-5; (5) $^{32}$P-ODN-5; and (6) Maxam-Gilbert G sequencing line of the $^{32}$P-ODN-5. The products of conjugation of DTPA with $NH_2$-ODN-1 are marked with arrows. Fragments that appeared as result of breaks are bracketed. (B) Distribution and relative intensity of breaks at individual bases of $^{32}$P-ODN-5 produced by $^{125}$I-NH-ODN-1 (white bars) and $^{111}$In-DTPA-NH-ODN-1 (dark bars). SDs, σ, are shown by vertical bars. Y indicates position of labeled residue.

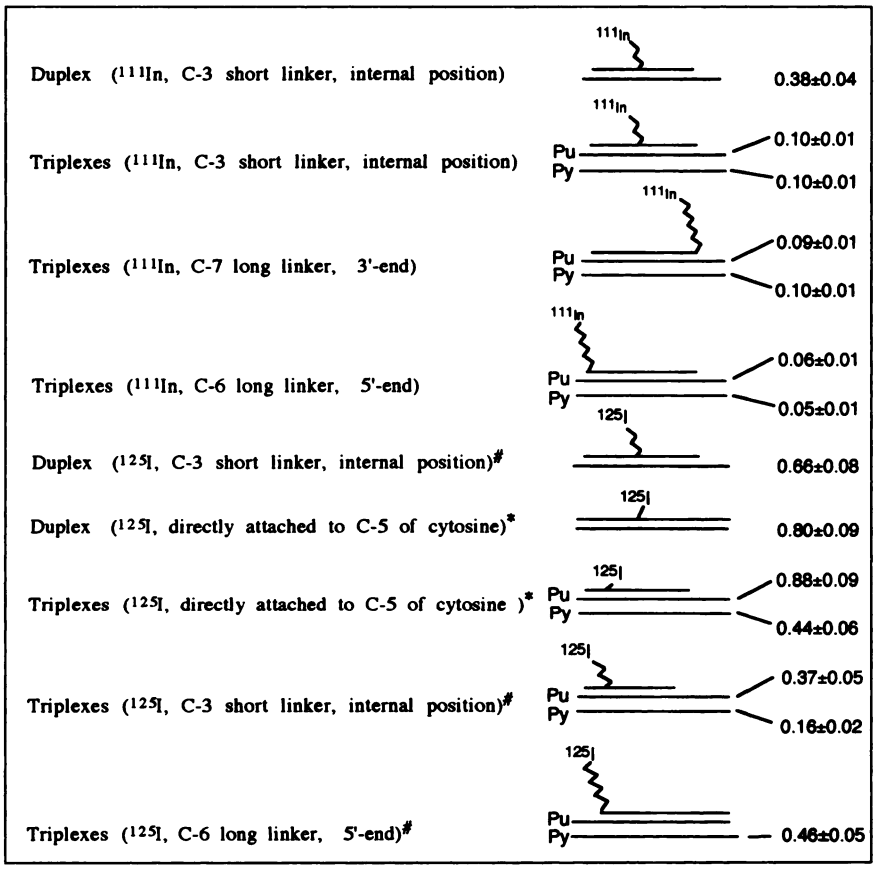


**FIGURE 4.** Yield of DNA strand breaks per decay of $^{111}$In and $^{125}$I. *Data from (*20*). #Data from (*26*).

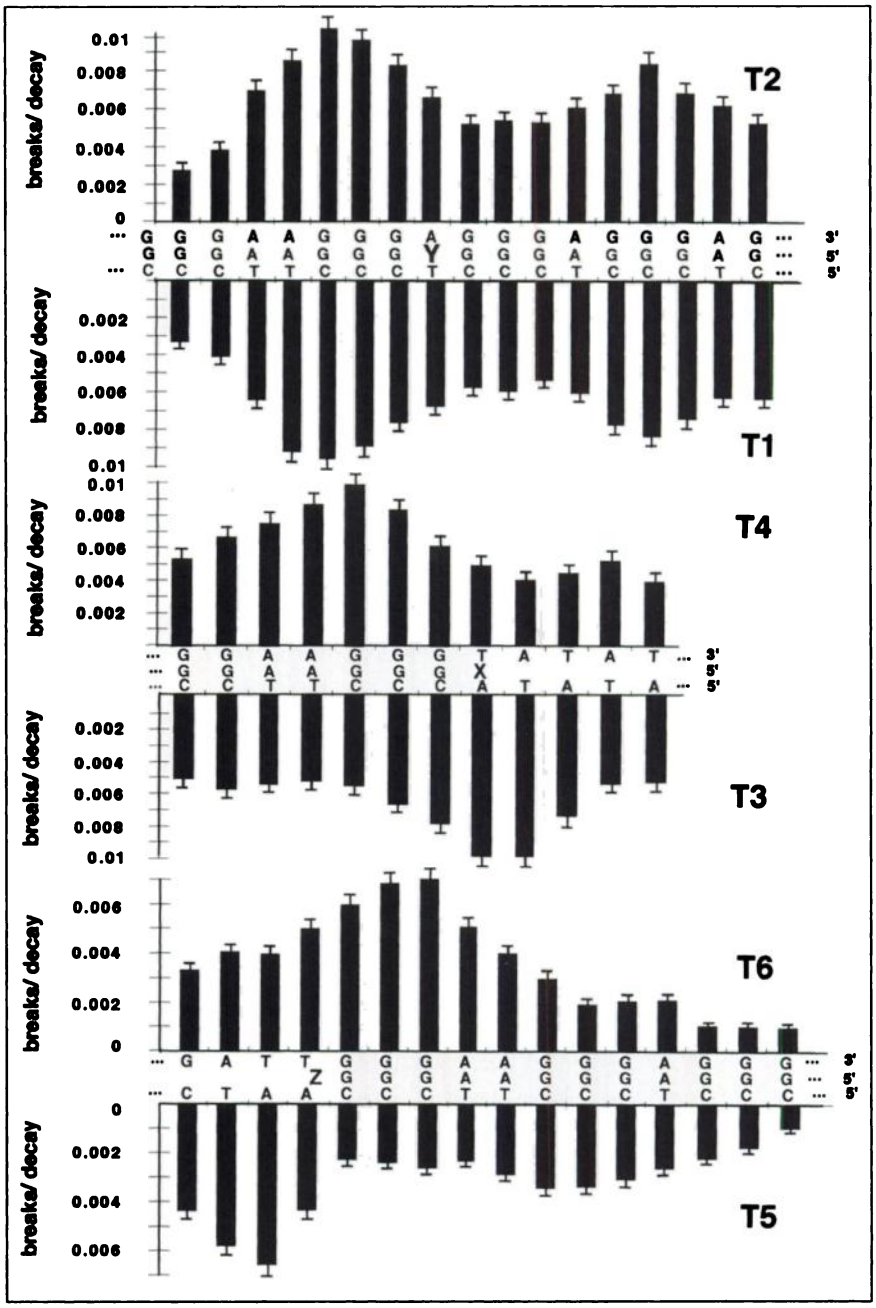


**FIGURE 5.** Distribution and relative intensity of breaks at individual bases in purine strand (triplexes T2, T4, T6) and pyrimidine strand (triplexes T1, T3, T5). Relative intensities are shown in same scale for purine and pyrimidine strand. SDs and σ are shown by vertical bars. X, Y, and Z indicate positions of $^{111}$In-labeled residues in the triplex triad.

toward the 5′ end of the target strand from the position of the attachment of the linker (Fig. 3B). The yield of strand breaks per decay of $^{111}$In for the duplex bearing the short internal linker (Fig. 1A) was nearly 2 times less than the yield of strand breaks per decay of $^{125}$I for the duplex bearing the same linker (Fig. 4).

### Breaks in a Duplex Produced by TFOs

Internally labeled triplex-forming $^{111}$In-DTPA-NH-ODN-2, 5′-end labeled $^{111}$In-DTPA-NH-ODN-3, or 3′-end labeled $^{111}$In-DTPA-NH-ODN-4 were synthesized from DTPA-NH-ODN(2-4) intermediates as describe above (Fig. 1). To form triplexes we used the same target sequence as in our previous study with $^{125}$I (*20*). $^{32}$P-ODN-6 and ODN-7 ($D_1$ duplex) or $^{32}$P-ODN-7 and ODN-6 ($D_2$ duplex) were annealed to form the target duplexes with the $^{111}$In-DTPA-NH-ODN(2–4) (Fig. 2).

Triplex formation between $^{111}$In-TFOs and the duplexes was confirmed by band shift in 20% native PAGE (Fig. 6). By measuring the intensities of the bands corresponding to the $^{32}$P-duplexes and $^{32}$P-triplexes, we calculated that 95% of the radioactivity for T3, T4, T5, and T6 triplexes; 47% for T1 triplex; and 27% for T2 triplex were associated with triplex structures. The triplex samples were kept for 12 d at −70°C for dose accumulation. After that time, the triplexes were disrupted by adding EDTA that chelated magnesium required for their stabilization. The samples were then

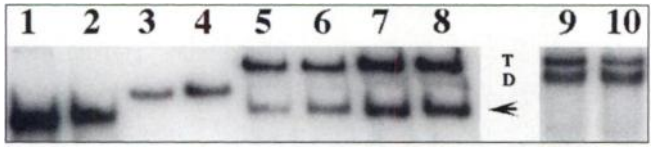


**FIGURE 6.** Analysis of triplex formation between $^{111}$In-DTPA-NH-ODN-2,3,4 and $^{32}$P-labeled duplexes in nondenaturating PAGE. Lanes: (1) $^{111}$In-DTPA-NH-ODN-3; (2) $^{111}$In-DTPA-NH-ODN-4; (3) duplex $D_1$ ($^{32}$P-ODN-6 + ODN-7); (4) duplex $D_2$ ($^{32}$P-ODN-7 + ODN-6); (5) triplex T5 ($^{111}$In-DTPA-NH-ODN-4 + duplex $D_1$); (6) triplex T6 ($^{111}$In-DTPA-NH-ODN-4 + duplex $D_2$); (7) triplex T3 ($^{111}$In-DTPA-NH-ODN-3 + duplex $D_1$); (8) triplex T4 ($^{111}$In-DTPA-NH-ODN-3 + duplex $D_2$); (9) triplex T1 ($^{111}$In-DTPA-NH-ODN-2 + duplex $D_1$); (10) triplex T2 ($^{111}$In-DTPA-NH-ODN-2 + duplex $D_2$). Arrow indicates position of $^{111}$In-labeled oligonucleotides. Positions of duplexes and triplexes are marked with D and T, respectively.

analyzed for fragmentation in 12% denaturing PAGE. The yields of the strand breaks for all the triplexes determined as described above for duplexes are summarized in Figure 4.

## DISCUSSION

The yield of ODN-targeted DNA strand breaks produced by the decay of $^{111}$In was determined as a function of the type of linker structure and its position. The simple and efficient method of the synthesis of $^{111}$In-labeled oligonucleotides with high specific activity from an amino-modified oligonucleotides was used. We showed that these labeled ODNs were able to form duplexes and triplexes with their complementary target sequences. The conditions of triplex formation used here were similar to our earlier studies of $^{125}$I-modified TFOs of the same sequences (*26*). The efficiencies of triplex formation at comparable concentrations in all cases were similar, or even better. Therefore, we deduce that $^{111}$In-bearing linkers do not impede triplex formation.

The yield of strand breaks per decay of $^{111}$In for the duplex bearing the short internal linker (Fig. 3B) was nearly 2 times less than the yield of strand breaks per decay of $^{125}$I for the duplex bearing the same linker. The difference in the yield of breaks clearly correlates with the difference in the calculated average energy deposited by the electrons in a unit density sphere 5 nm in radius around the decay sites of $^{111}$In and $^{125}$I (*16*). The break distribution for the $^{111}$In duplex was nearly the same as that for the $^{125}$I duplex.

In previous experiments we demonstrated that the yield of strand breaks produced by $^{125}$I strongly depends on the distance from the decay site to the DNA strand. It was shown that the 7 Å difference in distance from $^{125}$I to the DNA strands resulted in 4-fold lower yield of strand breaks (*20*). Therefore, for the calculation of probability of DNA strand breaks, one must take into account not only the average energy of the Auger electrons of $^{111}$In or $^{125}$I but also the distance from $^{125}$I or $^{111}$In atoms to the DNA strands. Unfortunately, there are no simple methods for synthesis of oligonucleotide derivatives with $^{111}$In directly attached to the base or ribose ring of the oligonucleotide to provide data for calculating probabilities of DNA strand breaks in relation to distance, as was done for $^{125}$I-DNA, triplex, or DNA-protein complexes (*20,27*). If the $^{111}$In or $^{125}$I were moved away from the DNA to the length of the fully extended linker, we could calculate the maximum distance from the radionuclides to the position of attachment of the linkers (11.3 Å for the short linker, $^{125}$I; 13.2 Å for the short linker, $^{111}$In; 15.6 Å for the long linker, $^{125}$I; 18 Å for the long linker, $^{111}$In) and, in principle, roughly estimate the relationship between the yield of DNA strand breaks and these distances.

Based on the position of the maxima of the distributions of strand cleavage, we can predict the position of $^{111}$In or $^{125}$I and speculate on the conformation of the linker. For example, for both isotopes tested, the maxima of the breaks distribution in 1 of the duplex DNA strands is shifted 4 bases to the 5′-end of the complementary strand from the linker-bearing base (Fig. 3B). According to x-ray data, the distance between the neighbor bases in B-DNA is 3.4 Å. Therefore, the distance between the first and the fifth bases should be 3.4 Å × 4 = 13.6 Å, which corresponds to the length of the fully extended linker (11.3 Å for the short linker, $^{125}$I; 13.2 Å for the short linker, $^{111}$In). This suggests that the linker "stretches" along the DNA duplex so that the distance between the ribose of the fifth nucleotide to the 5′-end and the radionuclide atom becomes the shortest distance. The data presented in Figure 4 show that there is a small difference in terms of the yield of DNA strand breaks per decay between the duplex where $^{125}$I is directly attached to the C-5 position of cytosine (0.8 breaks per decay) and the duplex where $^{125}$I is attached to the base through the short linker (0.66 breaks per decay). We can thus assume that the distances between the $^{125}$I or $^{111}$In and the nearest atoms of the ribose-phosphate backbone (the major target for Auger electrons [*28–31*]) are nearly the same. Therefore, we have good agreement between the probability of DNA breaks and the energy of the Auger electrons from $^{111}$In and $^{125}$I for the duplex-bearing isotopes on the short linker.

Although the mechanism of DNA cleavage by Auger electrons is complicated and not completely understood, it is commonly suggested that the main targets in the DNA molecule are deoxyriboses and phosphate groups (*28–31*). It is worth noting that the bands corresponding to $^{125}$I- and $^{111}$In-decay–induced breaks comigrate with the products of Maxam-Gilbert sequencing reaction and, therefore, may have the same chemical structure. Thus, the corresponding base and deoxyribose are completely eliminated, and the 5′-end of broken DNA has a terminal phosphate group (*22*).

The yield of DNA strand breaks in the pyrimidine and purine strands of the triplexes with $^{111}$In attached to the TFOs through the linkers of different length varies from 0.05 to 0.10 (Fig. 4). The yields of DNA strand breaks produced by $^{125}$I attached to the TFO through the linkers of the same length were 9-fold higher (pyrimidine strand, long linker, 5′-end) or 1.6-fold higher (pyrimidine strand, short linker, internal position) (Fig. 4). These differences in the yield of DNA strand breaks could be explained in terms of the surface charges of the triplex and $^{111}$In-DTPA linker.

Sahu et al. (*17*) have shown that formation of a negatively charged In-DTPA complex prevents the binding of In to DNA by ionic repulsion. Similarly, TFOs add more negative charge to the surface of the DNA, perhaps preventing the positioning of a $^{111}$In-DTPA group in close proximity to the major groove of DNA. Thus, we suggest that $^{111}$In-DTPA–bearing groups are positioned somewhere around the site of attachment at distances where ionic repulsion and steric hindrance become minimal; and, that the 2 maxima of breaks distribution of all triplexes tested most likely correspond to 2 different conformations of the linker relative to the DNA.

The breaks distribution, determined as described above, in both strands of the triplex with the internally labeled TFO is considerably wider (T1, T2, Fig. 5) than in the duplex with the same linker (Fig. 3B). These distributions have 2 maxima positions which coincide in the purine (T1) and the pyrimidine (T2) strands. The first pair of the maxima is shifted 3 nucleotides to the 3′-end of pyrimidine strand and to the 5′-end of the purine strand, and the second is shifted 6 nucleotides to the 5′-end of pyrimidine strand and to the 3′-end of purine strand relative to the position of the $^{111}$In-containing triad. The yield of the breaks in the first pair of maxima is somewhat stronger than in the other pair.

The positions of the maxima of breaks distribution in the pyrimidine and purine strands of the triplexes with $^{111}$In attached to the 5′-end of TFO do not coincide. The strongest maximum of breaks in the purine strand is shifted 2 nucleotides to the 5′-end, whereas in the pyrimidine strand it is shifted 1 nucleotide to the 5′-end relative to the position of $^{111}$In attachment (T4, T3, Fig. 5).

The strongest maximum of breaks in the purine strand of the triplex with $^{111}$In attached to the 3′-end of TFO is shifted 2 nucleotides to the 3′-end, whereas in the pyrimidine strand it is shifted 2 nucleotides to the 3′-end relative to the position of $^{111}$In-containing triad (T6, T5, Fig. 5).

## CONCLUSION

We have shown that $^{111}$In incorporated into duplex and triplex DNA structures in a sequence-specific manner produces DNA strand breaks in close proximity to the site of incorporation with an efficiency comparable with that of $^{125}$I. Our ability to produce $^{111}$In-TFO conjugates with a high specific activity makes them very promising agents for trials of antigene radiotherapy. As with $^{125}$I (*14*), $^{111}$In becomes an AE radionuclide that can be shown experimentally to produce highly localized damage when positioned close to DNA. $^{111}$In can thus be considered for many of the therapeutic applications that have been proposed for $^{125}$I (*4*), with the great advantage of having photons for scintigraphy and a considerably shorter half-life. It may also be important to consider DNA binding by $^{111}$In-labeled radiopharmaceuticals used in nuclear medicine for more accurate calculations of their dosimetry, as was pointed out earlier for $^{125}$I (*16,32*).


## ACKNOWLEDGMENTS

The authors thank William Eckelman and Ludvig Feinendegen for many fruitful discussions and helpful suggestions.


## REFERENCES


1. Carlson TA, White RM. Formation of fragment ions from $CH_3Te^{125}$ and $C_2H_5Te^{125}$ following the nuclear decays of $CH_3I^{125}$ and $C_2H_5I^{125}$. *J Chem Phys.* 1963;38:2930–2934.
2. Feinendegen LE. Biological damage from the Auger effect, possible benefits. *Radiat Environ Biophys.* 1975;12:85–99.
3. Sastry KS. Biological effects of the Auger emitter iodine-125: a review. Report no. 1 of the AAPM Nuclear Medicine Task Group No. 6 [see comments]. *Med Phys.* 1992;19:1361–1370.
4. Adelstein SJ. The Auger process: a therapeutic promise? *AJR.* 1993;160:707–713.
5. Halpern A, Stocklin G. Chemical and biological consequences of beta-decay. Part 2. *Radiat Environ Biophys.* 1977;14:257–274.
6. Jiang VW, Welch MJ. Intramolecular effects of $^{125}$I decay in 3-iodotyrosine. *Radiat Res.* 1977;69:16–26.
7. Panyutin IG, Neumann RD. Gene radiotherapy; gene targeted versus targeted by gene product. *J Nucl Med.* 1998;39:928–929.
8. Frank-Kamenetskii MD, Mirkin SM. Triplex DNA structures. *Annu Rev Biochem.* 1995;64:64–95.
9. Felsenfeld GR, Rich A. Studies on the formation of two- and three-stranded polyribonucleotides. *Biochim Biophys Acta* 1957;26:457–463.
10. Helene C. The anti-gene strategy: control of gene expression by triplex-forming-oligonucleotides. *Anticancer Drug Design.* 1991;6:569–584.
11. Giovannangeli C, Thuong N, Helene C. Oligodeoxynucleotide-directed photo-induced cross-linking of HIV proviral DNA via triple-helix formation. *Nucleic Acids Res.* 1992;20:4275–4281.
12. Shimizu M, Inoue H, Ohtsuka E. Detailed study of sequence-specific DNA cleavage of triplex-forming oligonucleotides linked to 1,10-phenanthroline. *Biochemistry.* 1994;33:606–613.
13. Panyutin IG, Neumann RD. Sequence-specific DNA double-strand breaks induced by triplex forming $^{125}$I labeled oligonucleotides. *Nucleic Acids Res.* 1994;22:4979–4982.
14. Martin RF, Haseltine WA. Range of radiochemical damage to DNA with decay of iodine-125. *Science.* 1981;213:896–898.
15. Dewanjee MK, Ghafouripour AK, Kapadvanjwala M, et al. Noninvasive imaging of c-myc oncogene messenger RNA with indium-111-antisense probes in a mammary tumor-bearing mouse model [see comments]. *J Nucl Med.* 1994;35:1054–1063.
16. Sastry KS, Howell RW, Rao DV, et al. Dosimetry of Auger emitters: physical and phenomenological approaches. In: Baverstock KF, Charlton DE, eds. *DNA Damage by Auger Emitters.* London, UK: Taylor & Francis;1988:27–38.
17. Sahu SK, Kassis AI, Makrigiorgos GM, et al. The effects of indium-111 decay on pBR322 DNA. *Radiat Res.* 1995;141:193–198.
18. Gamper HB, Reed MW, Cox T, et al. Facile preparation of nuclease resistant 3′ modified oligodeoxynucleotides. *Nucleic Acids Res.* 1993;21:145–150.
19. Tabone JC, Stamm MR, Gamper HB, et al. Factors influencing the extent and regiospecificity of cross-link formation between single-stranded DNA and reactive complementary oligodeoxynucleotides. *Biochemistry.* 1994;33:375–383.
20. Panyutin IG, Neumann RD. Radioprobing of DNA: distribution of DNA breaks produced by decay of $^{125}$I incorporated into a triplex-forming oligonucleotide correlates with geometry of the triplex. *Nucleic Acids Res.* 1997;25:883–887.
21. Cooney M, Czernuszewicz G, Postel EH, et al. Site-specific oligonucleotide binding represses transcription of the human c-myc gene in vitro. *Science.* 1988;241:456–459.
22. Maxam AM, Gilbert W. Sequencing end-labeled DNA with base-specific chemical cleavages. *Methods Enzymol.* 1980;65:499–525.
23. Hnatowich DJ, Winnard P Jr, Virzi F, et al. Technetium-99m labeling of DNA oligonucleotides. *J Nucl Med.* 1994;36:2306–2314.
24. Hnatowich DJ, Layne WW, Childs RL, et al. Radioactive labeling of antibody: a simple and efficient method. *Science.* 1983;220:613–615.
25. Paik CH, Murphy PR, Eckelman WC, et al. Optimization of the DTPA mixed-anhydride reaction with antibodies at low concentration. *J Nucl Med.* 1983;24:932–936.
26. Karamychev VN, Panyutin IG, Reed MW, Neumann RD. Effect of radionuclide linker structure on DNA cleavage by $^{125}$I-labeled oligonucleotides. *Antisense Nucleic Acid Drug Dev.* 1997;7:549–557.

27. Karamychev VN, Zhurkin VB, Garges S, Neumann RD, Panyutin IG. Detecting the DNA kink in a DNA-CRP complex in solution with iodine-125 radioprobing. *Nat Struct Biol.* 1999;6:747–750.
28. Charlton DE, Humm JL. A method of calculating initial DNA strand breakage following the decay of incorporated $^{125}$I. *Int J Radiat Biol.* 1988;53:353–365.
29. Pomplun E. A new DNA target model for track structure calculations and its first application to I-125 Auger electrons. *Int J Radiat Biol.* 1991;59:625–642.
30. Terrissol M. Modelling of radiation damage by $^{125}$I on a nucleosome. *Int J Radiat Biol.* 1994;66:447–451.
31. Nikjoo H, O'Neill P, Terrissol M, et al. Modelling of radiation-induced DNA damage: the early physical events. *Int J Radiat Biol.* 1994;66:453–457.
32. Sedelnikova OA, Panyutin IG, Thierry AR, Neumann RD. Radiotoxicity of iodine-125-labeled oligodeoxyribonucleotides in mammalian cells. *J Nucl Med.* 1998;39:1412–1418.